Automatic Flux-Weakening Control of Permanent Magnet Synchronous Motors Using a Reduced-Order Controller

Jiunn-Jiang Chen and Kan-Ping Chin, *Member, IEEE*

***Abstract*—This study presents a novel means of designing a simple and effective position and velocity controller for permanent magnet synchronous motors (PMSM). In contrast to the conventional two-loop control methods with full-state feedback, the proposed controller does not need current information of the motor for feedback purposes. However, under normal operation the steady-state d-axis current can still be controlled to zero to minimize power dissipation. In addition, implementing a simple overmodulation strategy allows the controller to automatically generate a flux-weakening control to expand the range of operating speed when voltage saturation occurs. In addition to not depending on system parameters used by the controller, the automatically generated demagnetizing current is also optimal in the sense of minimum power dissipation that differs from the maximum output torque design or the constant power design of the general flux-weakening control methods. Simulation and experimental results show that the controller can achieve an effective speed and position control with near-minimum power dissipation, even when voltage saturation occurs.**

***Index Terms*—Feedback, flux-weakening control methods, PMSM, torque.**

I. Introduction

RECENT advances in power electronics and high-speed microprocessors have led to considerable attention in applying nonlinear control theory to electronically-commutated alternate current (ac) electrical machines. In general, the mathematical model of an ac motor consists of coupled high-order nonlinear ordinary differential equations representing the dynamics of electrical and mechanical subsystems. Hence, a fully digitally controlled ac motor is a multiinput nonlinear system where the inputs are the phase voltages and the outputs are the position, the velocity or the torque at the rotor shaft. Recent developments in nonlinear system analyzes and control technologies suggest that the controllers for electrical motors should be designed directly from nonlinear models. To simplify controller design, the two-loop control method [1], as shown in Fig. 1, is the most frequently applied in small electrical machine control. Sliding mode control has also been applied to the control of electrical machines, such as induction motors [2] and synchronous motors [3]. More recently, feedback linearization techniques have been extensively applied to the control of variable reluctance motors [4], permanent magnet synchronous motors (PMSM) [5], induction motors [6], and hybrid motors [7], [8]. Other investigations have applied adaptive control with feedback linearization terms in various motors [9]–[11]. Although these nonlinear control technologies can be used for variable speed control design, intensive computations and full-state feedback, including position, velocity and phase currents, are required for such implementation.

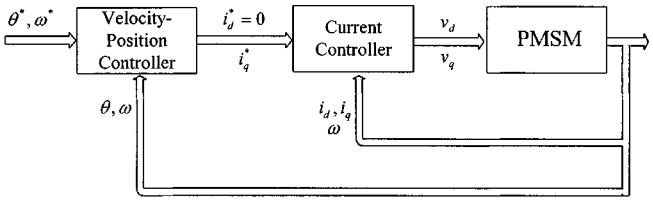

Fig. 1. Block diagram of a two-loop control system for the PMSM.

Another relevant topic of motor controls is how to extend the speed ranges. As it rises with an increasing speed, the back emf cancels a portion of the input voltages and limits the injected currents, thus restricting the maximum speed of the motor to a certain level. To extend the range of operational speed of the motor, many authors have proposed different algorithms to accomplish flux-weakening control [12]–[17]. Flux-weakening control of PMSM's employs a negative d-axis current (demagnetizing current) to suppress the back emf. References [12]–[15] proposed several flux-weakening controls of PMSM's. In these methods, a d-axis current command is determined to achieve maximum torque output or constant power output. However, these methods are extremely sensitive to the accuracy of the motor parameters used in controllers. References [16], [17] presented flux-weakening control methods that do not require knowledge of the load torque or motor parameters. A method is that in which the d-axis current command is proportional to the filtered q-axis current error [16]. Another method is that in which the d-axis current command is adjusted by taking a PI control of the voltage error between the saturated voltage and the output voltage command of current controller [17]. However, for both of these flux-weakening control methods, the control stability in flux-weakening regions always depends on the choices of the control gains which are used to tune the d-axis current command. Consequently, how to select control gains is of primary concern when implementing these two flux-weakening control methods.

In this study, we present a nonlinear reduced-order model for a PMSM by approximating the original full-order model using

Manuscript received October 25, 1999; revised May 30, 2000. Recommended by Associate Editor J. Ojo.

The authors are with the Department of Mechanical Engineering, National Chiao-Tung University, Hsinchu 30010, Taiwan R.O.C. (e-mail: kanping@cc.nctu.edu.tw).

Publisher Item Identifier S 0885-8993(00)07313-0.

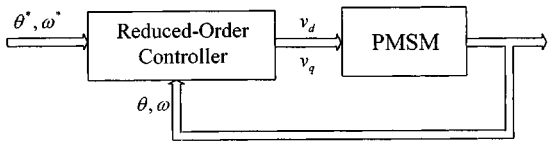

Fig. 2. Block diagram of a reduced-order control system for the PMSM.

a singular perturbation method [18], [19]. The motivation behind doing so is to exploit the two-time-scale properties of small electrical machines where the mechanical subsystem is significantly slower than the electrical subsystem. Under such circumstances, the mechanical variables in the electrical subsystem are regarded as frozen and the electrical variables in the mechanical subsystem are regarded as capable of instantaneously arriving at their quasisteady-state. Consequently, the electrical variables can be expressed as functions of the mechanical variables; a reduced-order dynamic model that only consists of the mechanical variables is derived as well. The resulting reduced model of the PMSM is accurate enough to capture the dominant dynamic behavior of the PMSM, and can be used to develop effective nonlinear PMSM reduced-order controllers. Fig. 2 schematically depicts a reduced-order control system.

Because this reduced-order model is a second-order nonlinear system, many standard nonlinear and adaptive control techniques can be applied to the design of the controllers. Moreover, with this control methodology, the current measurement, which is sensitive to noise corruption and required in any full-state feedback controller, can be eliminated. Although phase currents are not measured for control purposes, the steady-state d-axis current can still be indirectly controlled to zero under normal operation to achieve near-minimum power dissipation. Furthermore, implementing an overmodulation strategy allows the controller to automatically generate a demagnetizing current to expand the speed range when input voltage saturation occurs. This flux weakening control is also optimal in the sense of minimum power dissipation, and differs from the maximum output torque design or the constant power design in the general flux-weakening control methods [12]–[15]. Stability analyzes based on the Lyapunov's linearization method indicate that, to stabilize the closed-loop system, the control gains in the reduced controller must be both upper and lower bounded. In addition, when voltage saturation occurs, the closed-loop system is still stable, as long as the degree of saturation is not too much. Simulation and experiments are performed to verify the performance of the proposed controller. According to those results, the proposed controller can achieve an effective position and velocity control with near-minimum power dissipation, even when voltage saturation occurs.

The rest of this paper is organized as follows. Section II presents the mathematical model of a PMSM. In Section III, we derive a reduced model using the singular perturbation method. The reduced controller based on this reduced model, as well as the overmodulation strategy that we have adopted is also described. Section IV describes the stability analyzes. Sections V and VI summarize the simulation and experimental results, respectively. Conclusions are finally made in Section VII.

II. Motor Model

The mathematical model of a surface permanent magnet synchronous motor (SPMSM) in a synchronous frame, or the so-called d–q frame, can be described as follows:

$$\dot{\boldsymbol{x}} = \begin{Bmatrix} \dot{\theta} \\ \dot{\omega} \end{Bmatrix} = \begin{Bmatrix} \omega \\ [3/2KNi_q - B\omega - C\text{sgn}(\omega)]/J \end{Bmatrix} \tag{1}$$

$$\dot{\boldsymbol{i}} = \begin{Bmatrix} \dot{i}_d \\ \dot{i}_q \end{Bmatrix} = \begin{bmatrix} -R/L & N\omega \\ -N\omega & -R/L \end{bmatrix} \begin{Bmatrix} i_d \\ i_q \end{Bmatrix} + \frac{1}{L} \begin{Bmatrix} v_d \\ v_q - KN\omega \end{Bmatrix} \tag{2}$$

where

$\boldsymbol{x} = \{\theta\ \omega\}^T$	mechanical state vector whose components are the rotor position and rotor velocity, respectively;
$\boldsymbol{i} = \{i_d\ i_q\}^T$	electrical state vector in the d–q frame, and the components of i are the direct and the quadrature-axis stator currents respectively;
$\boldsymbol{v} = \{v_d\ v_q\}^T$	input vector whose components are input voltages in the d–q frame;
L	phase inductance;
R	phase resistance;
N	number of pole pair;
K	torque (permanent magnet) constant;
J	rotor inertia;
B	viscous damping coefficient;
C	Coulomb friction coefficient.

Owing to that this study focuses on achieving position or velocity controls without using the current information, the input voltage is constrained to a function of time and the mechanical states, $\boldsymbol{v} = \boldsymbol{v}(t, \boldsymbol{x})$.

III. Control Strategies

A. Reduced Order Modeling

The two-time-scale phenomenon of small electrical machines is manifested by the fact that the time constant of the electrical subsystem, L/R, is significantly smaller than that of the mechanical subsystem, J/B. Hence, assigning a small positive constant $\varepsilon = L/R$ allows us to rewrite the motor model (1), (2) into a standard singular perturbation model [18], [19] by multiplying ε to both sides of the electrical subsystem (2)

$$\begin{Bmatrix} \dot{\theta} \\ \dot{\omega} \end{Bmatrix} = \begin{Bmatrix} \omega \\ \dfrac{3KN}{2J} i_q - \dfrac{B}{J}\omega - \dfrac{C}{J}\text{sgn}(\omega) \end{Bmatrix} \tag{3}$$

$$\varepsilon \begin{Bmatrix} \dot{i}_d \\ \dot{i}_q \end{Bmatrix} = \begin{bmatrix} -1 & LN\omega/R \\ -LN\omega/R & -1 \end{bmatrix} \begin{Bmatrix} i_d \\ i_q \end{Bmatrix} + \frac{1}{R} \begin{Bmatrix} v_d \\ v_q - KN\omega \end{Bmatrix}. \tag{4}$$

Notably, in (4), although L/R is a small number, the term $LN\omega/R$ may not be a small one when $N\omega$ is large. Therefore, $LN\omega/R$ cannot be considered as a negligible parasitic term.

Suppose the fast subsystem (4) reaches its quasisteady-state instantaneously when the electrical time constant is significantly smaller than the mechanical time constant. The quasisteady-

state of the electrical variables can be determined by substituting $\varepsilon = 0$ in (4)

$$\begin{Bmatrix} \bar{i}_d \\ \bar{i}_q \end{Bmatrix} = \frac{1}{DL} \begin{Bmatrix} (v_q - KN\omega)N\omega + Rv_d/L \\ -(v_d + KR/L)N\omega + Rv_q/L \end{Bmatrix} \quad (5)$$

where $D = N^2\omega^2 + R^2/L^2$, and $\bar{i}_d$ and $\bar{i}_q$ are the quasisteady-state values of i_d and i_q, respectively. By replacing i_q in (3) with its quasisteady-state $\bar{i}_q$, a reduced model of the full system (3), (4) is obtained

$$\begin{Bmatrix} \dot{\theta} \\ \dot{\omega} \end{Bmatrix} = \begin{Bmatrix} \omega \\ \dfrac{3KN}{2J}\bar{i}_q - \dfrac{B}{J}\omega - \dfrac{C}{J}\,\mathrm{sgn}(\omega) \end{Bmatrix}. \quad (6)$$

The reduced model (6) is described by a set of nonlinear second-order differential equations in which the states are the same as the states of the mechanical subsystem in the full mode (3), (4). For further development, we let $e_\theta = \theta - \theta^*$, $e_\omega = \omega - \omega^*$, and $\boldsymbol{e_x} = \{e_\theta\ e_\omega\}^T$, where θ^* and ω^* are the desired position and the desired velocity respectively.

B. Control Law Design

Let $\bar{i}_d^*$ be the desired steady-state d-axis current. The relationship between v_d and v_q that produces this steady-state d-axis current can be solved from (5) as follows:

$$v_d = \frac{L}{R}[DL\bar{i}_d^* + N\omega(KN\omega - v_q)]. \quad (7)$$

By substituting (7) into (5), $\bar{i}_q$ becomes

$$\bar{i}_q = \frac{1}{R}[-N\omega(L\bar{i}_d^* + K) + v_q]. \quad (8)$$

Furthermore, the reduced model (6) can be rewritten as the following form by substituting (8) into (6):

$$v_q = \frac{2JR}{3KN}\dot{\omega} + \left[\frac{2BR}{3KN} + N(L\bar{i}_d^* + K)\right]\omega + \frac{2CR}{3KN}\,\mathrm{sgn}(\omega). \quad (9)$$

Based on (9), a feedback linearization control law can be chosen as follows:

$$v_q = \frac{2JR}{3KN}(\dot{\omega}^* - f) + \left[\frac{2BR}{3KN} + N(L\bar{i}_d^* + K)\right]\omega + \frac{2CR}{3KN}\,\mathrm{sgn}(\omega) \quad (10)$$

where $f = \lambda_\omega e_\omega + \lambda_\theta e_\theta + \lambda_\varphi e_\varphi$, $e_\varphi = \int e_\theta\, dt$, and λ_ω, λ_θ and λ_φ are control gains. By substituting the control laws (10) into the reduced model (9), the closed-loop error dynamics becomes

$$\begin{cases} \dot{e}_\varphi = e_\theta \\ \dot{e}_\theta = e_\omega \\ \dot{e}_\omega = -f \end{cases}. \quad (11)$$

By selecting the control gains as $\lambda_\omega = \sigma_a + \sigma_b + \sigma_c$, $\lambda_\theta = \sigma_a\sigma_b + \sigma_b\sigma_c + \sigma_a\sigma_c$, and $\lambda_\varphi = \sigma_a\sigma_b\sigma_c$, we can assign the eigenvalues of the closed-loop error dynamics (11) to $-\sigma_a$, $-\sigma_b$ and $-\sigma_c$. Consequently, the equilibrium point of the reduced model (6) is globally exponentially stable under the control law (7) and (10), as long as the control gains, $(\lambda_\omega,\ \lambda_\theta,\ \lambda_\varphi)$, or equivalently, the real part of the values, $(\sigma_a,\ \sigma_b,\ \sigma_c)$, are all positive.

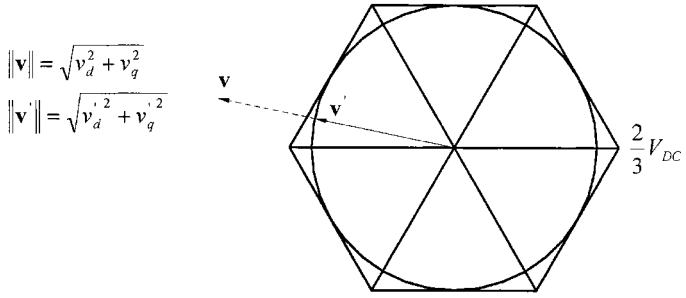

Fig. 3. Adopted overmodulation strategy.

C. Overmodulation Strategy

Overmodulation occurs when the magnitude of the command voltage is greater than the saturated voltage, which is the maximum magnitude of the output voltage of an inverter, and is limited by the inverter dc link voltage. The inverter dc link voltage is denoted as V_{DC}. An overmodulation strategy determines the actual output voltage vector when overmodulation occurs [20]. In this study, the overmodulation strategy is chosen so that when the magnitude of the command voltage vector exceeds the saturated voltage, the magnitude of the command voltage vector is shrunk to be equal to the saturated voltage; meanwhile, the angle of the command voltage vector remains unchanged. The overmodulation strategy can be described as follows:

$$v_d' = \rho v_d \quad (12)$$

$$v_q' = \rho v_q \quad (13)$$

where

$$\rho = V_{sat} \Big/ \sqrt{v_d^2 + v_q^2}, \qquad 0 < \rho < 1 \quad (14)$$

is a scaling factor for the output voltages when the saturation occurs, V_{sat} denotes the magnitude of the saturated voltage, and v_d' and v_q' represent the actual output voltages after scaling. Fig. 3 illustrates the adopted overmodulation strategy. Theoretically, the boundary of all saturated voltage vectors of a PWM inverter will form a hexagon. In this study, the hexagon is replaced by a circle as the boundary of all saturated voltage vectors for convenience. Under such a condition, the relation between the actual output voltage and the saturated voltage can be described by the following equation:

$$v_d'^2 + v_q'^2 = V_{sat}^2 \quad (15)$$

where the magnitude of the saturated voltage is a constant value and can be expressed as $V_{sat} = V_{\mathrm{DC}}/\sqrt{3}$.

IV. Stability Analyses

In the previous section, control laws (7) and (10) are designed to stabilize the reduced model, which assumes that the fast (electrical) subsystem reaches its quasisteady-state instantaneously. Nevertheless, (7) and (10) will also stabilize the original full system as demonstrated hereinafter. In this section, we analyze the stability of the closed-loop full system under both normal operating condition and voltage saturation condition using the Lyapunov's linearization method.

TABLE I
THE RATINGS AND IDENTIFIED PARAMETERS OF THE SINANO #7CB30-2SE6F MOTOR

Ratings	$P_{rated} = 300[W], V_{rated} = 200[V],$ $\omega_{rated} =$ [rpm], $I_{phase\_rated} = 2[A], I_{phase\_peak} = 6[A].$
Pole pair	$N = 4$
Resistance	$R = 3.55[\Omega]$
Inductance	$L = 5.92 \times 10^{-3}$ [H]
Magnet constant	$K = 5.795 \times 10^{-2}$ [V · sec/rad]
Rotor inertia	$J = 6.45 \times 10^{-5}$ [kg · m^2]
Viscous damping coefficient	$B = 8 \times 10^{-5}$ [N · m · sec/rad]
Column friction coefficient	$C = 1.738 \times 10^{-2}$ [N · m]

A. Normal Operation

Because the d-axis current, i_d, does not generate torque in a SPMSM system, it is commanded to become zero under normal operating conditions to reduce the power dissipation from the winding resistance. However, because i_d is not a state in the reduced model, to achieve near minimum power dissipation in this study, we will let $\bar{i}_d^* = 0$ instead. By substituting (7) and (10) with $\bar{i}_d^* = 0$ and ω^* be a constant into the original model (1) and (2), the closed-loop error dynamics of the full system becomes

$$\begin{cases} \dot{e}_\varphi = e_\theta \\ \dot{e}_\theta = e_\omega \\ \dot{e}_\omega = \dfrac{3KN}{2J}\tilde{i}_q - f \\ \dot{\tilde{i}}_d = -\dfrac{R}{L}\tilde{i}_d + N(e_\omega + \omega^*)\tilde{i}_q \\ \dot{\tilde{i}}_q = -N(e_\omega + \omega^*)\tilde{i}_d - \dfrac{R}{L}\tilde{i}_q - \dfrac{2B}{3KN}\dot{e}_\omega + \dfrac{2J}{3KN}\dot{f} \end{cases} \tag{16}$$

where $\tilde{i}_d = i_d - \bar{i}_d$ and $\tilde{i}_q = i_q - \bar{i}_q$. The system described by (16) is an autonomous system, and its origin is a unique equilibrium point. Consequently, the asymptotic stability of (16) also indicates the control goals, $e_\theta = 0$, $e_\omega = 0$, and $\tilde{i}_d = i_d - \bar{i}_d = _d = 0$, are achieved. The local stability of the system (16) can be analyzed by linearizing (16) around its equilibrium point. The parameters of the motor listed in Table I are employed in the following eigenvalue analyzes. Fig. 4(a)–(c) illustrate the loci of eigenvalues of (16) by varying ω^* from 10 to 4000 rpm. On the other hand, the equivalent control gains are chosen to have equal values, $\sigma_a = \sigma_b = \sigma_c$, at $5 \times 2\pi$, $35 \times 2\pi$, and $60 \times 2\pi$ for Fig. 4(a)–(c), respectively. One set of two loci on the left-hand side of Fig. 4(a) consists of eigenvalues of the electrical subsystem, and the other set of three loci on the right-hand side of Fig. 4(a) consists of eigenvalues of the mechanical subsystem. In Fig. 4(b) and (c), where the equivalent control gains are increased to $35 \times 2\pi$ and $60 \times 2\pi$, respectively, the set of loci representing eigenvalues of the electrical subsystem moves toward the imaginary axis and to the right of the set of loci representing eigenvalues of the mechanical subsystem. Furthermore, when the equivalent control gains are further increased to above a certain value, the set of loci representing eigenvalues of the electrical system moves into the right-half plane and the system becomes unstable. From this, we can infer that the control gains in (10), which was developed from the reduced model, not only needs to be lower-bounded, but also upper-bounded to stabilize the full model.

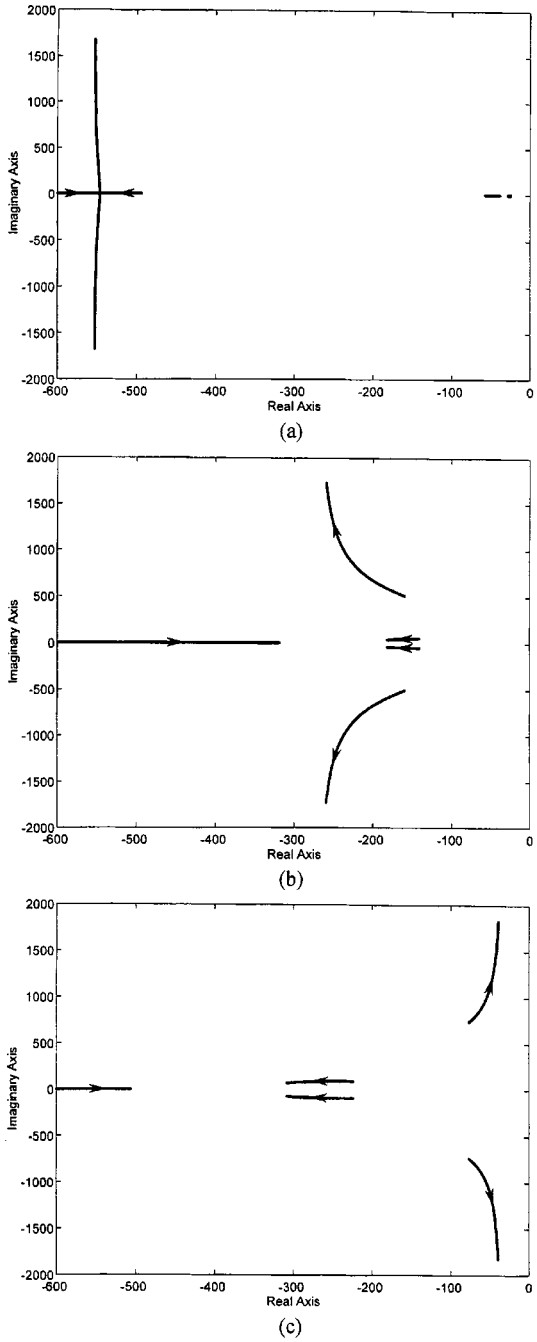

Fig. 4. Loci of eigenvalues when $\omega^* = 10 \sim 4000$ rpm and (a) $\sigma_a = \sigma_b = \sigma_c = 5 \times 2\pi$, (b) $\sigma_a = \sigma_b = \sigma_c = 35 \times 2\pi$, and (c) $\sigma_a = \sigma_b = \sigma_c = 60 \times 2\pi$.

B. Voltage Saturation Operation

During the control of an electrical motor, the back emf, which is proportional to the speed of the motor, cancels the input voltage and restricts the motor speed to a certain value corresponding to a given input voltage level. When the input voltage reaches the saturation voltage of the inverter, the motor reaches its maximum speed unless a demagnetizing current is generated to achieve the so-called flux-weakening control. In terms of speed control, the motor may even become unstable if the flux-weakening control is not implemented and the desired motor speed requires an input voltage level that exceeds the saturation voltage. In this study, because the current is only indirectly controlled in the reduced controller, what happens to the overall closed-loop system when the voltage saturation occurs is of interest. Let $\bar{i}_d^*$ be zero and ω^* be kept at a constant speed as before. When the voltage saturation occurs, the actual output voltages are expressed as in (12) and (13). By substituting (12), (13) and the control law (7) and (10) into the original full model (1) and (2), the closed-loop error dynamics becomes

$$\begin{cases} \dot{e}_\phi = e_\theta \\ \dot{e}_\theta = e_\omega \\ \dot{e}_\omega = \dfrac{3KN}{2J}\tilde{i}_q - \rho[(\sigma_a+\sigma_b+\sigma_c)e_\omega \\ \qquad +(\sigma_a\sigma_b+\sigma_c\sigma_a+\sigma_b\sigma_c)e_\theta \\ \qquad +\sigma_a\sigma_b\sigma_c(e_\phi+\varphi_c)] \\ \quad +(\rho-1)\left[\dfrac{B}{J}(e_\omega+\omega^*)+\dfrac{C}{J}\,\mathrm{sgn}(e_\omega+\omega^*)\right. \\ \qquad \left.+\dfrac{R}{DL^2}\dfrac{3K^2N^2}{2J}(e_\omega+\omega^*)\right] \\ \dot{\tilde{i}}_d = -\dfrac{R}{L}\tilde{i}_d + N(e_\omega+\omega^*)\tilde{i}_q - \dot{\bar{i}}_d \\ \dot{\tilde{i}}_q = -N(e_\omega+\omega^*)\tilde{i}_d - \dfrac{R}{L}\tilde{i}_q - \dot{\bar{i}}_q \end{cases} \tag{17}$$

where $e_\phi = e_\varphi - \varphi_c$, $\varphi_c = \varphi_c(\rho_{eq}, \omega^*)$ is a constant, and ρ_{eq} is the scaling factor at the equilibrium point of (17). By translating the coordinate axis e_φ of the system (16) to e_ϕ in (17), the equilibrium point is moved to the origin of (17). Consequently, the asymptotic stability of (17) also indicates the control goals, $e_\theta = 0$, $e_\omega = 0$, and $\tilde{i}_d = i_d - \bar{i}_d = 0$, are achieved. As in the previous section, the system described by (17) is linearized around its equilibrium point to analyze the stability of (17). Fig. 5 illustrates the loci of eigenvalues of (17) by setting the three equivalent control gains at $\sigma_a = \sigma_b = \sigma_c = 35 \times 2\pi$, and by varying ω^* from 10–4000 rpm. Moreover, Fig. 5(a) and (b) illustrate the loci of eigenvalues corresponding to the conditions when the scaling factor at equilibrium point is $\rho_{eq} = 0.5$ and $\rho_{eq} = 0.3$, respectively. Notably, the loci of eigenvalues plotted in Fig. 4(b) are equivalent to the loci of eigenvalues when $\rho_{eq} = 1$. These figures reveal that, when the value of ρ_{eq} decreases, the set of loci representing eigenvalues of the mechanical subsystem moves to the right of the pole plane. These results indicate that the closed-loop system operating under the voltage saturation region is stable as long as the degree of saturation is not too much. Moreover, following the loci of eigenvalues move toward the imaginary axis, the settling time of the responses under voltage saturation operation is longer than that under normal operations. The longer settling time implies that the controller under voltage saturation operation has weaker abilities of trajectory tracking and disturbance rejection. Based on these analysis results, an additional control strategy is proposed in the Experimental Section to reduce these drawbacks.

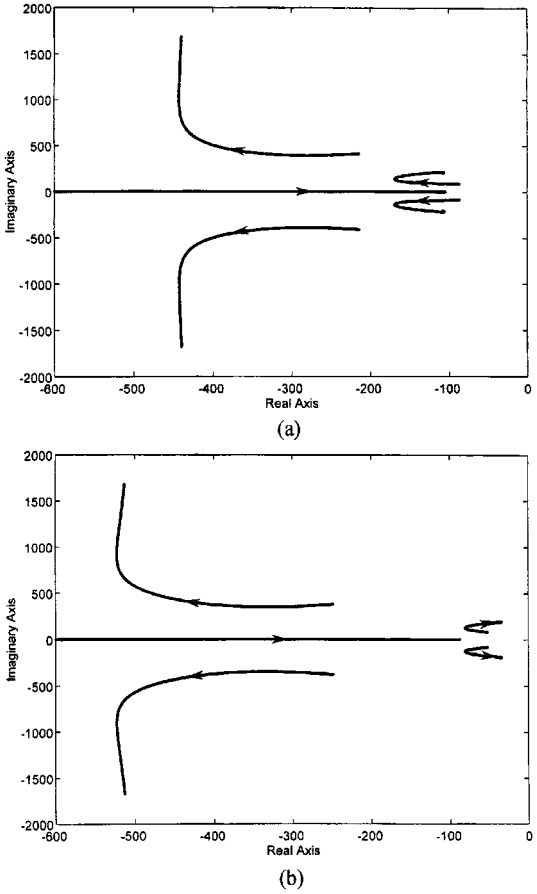

Fig. 5. Loci of eigenvalues when $\omega^* = 10 \sim 4000$ rpm, $\sigma_a = \sigma_b = \sigma_c = 35 \times 2\pi$: (a) $\rho_{eq} = 0.5$ and (b) $\rho_{eq} = 0.3$.

Also of relevant interest is how voltage saturation affects the values of the d–q currents. By substituting the overmodulation rules (12) and (13) into (5), the quasisteady-state d-axis current under voltage saturation, $\bar{i}_{d,\,sat}$, becomes

$$\bar{i}_{d,\,sat} = \frac{1}{DL}KN^2\omega^2(\rho-1) < 0. \tag{18}$$

Because $\bar{i}_{d,\,sat}$ is always less than zero when $\rho < 1$, it is a demagnetizing current that realizes flux-weakening control automatically when voltage saturation occurs. Moreover, the scaling factor at equilibrium can be derived from (15) as

$$\rho_{eq} = \sqrt{\frac{V_{sat}^2 - \dfrac{(L^2N^2\omega^{*2}+R^2)A^2}{R^2}}{K^2N^2\omega^{*2}\left(1-\dfrac{R^2}{L^2N^2\omega^{*2}+R^2}\right)}} \tag{19}$$

where

$$A = \left[\left(\frac{2BR}{3KN} + \frac{KNR^2}{(L^2N^2\omega^{*2}+R^2)}\right)\omega^* + \frac{2CR}{3KN}\mathrm{sgn}(\omega^*)\right].$$

Consequently, by substituting (19) into (18), $\bar{i}_{d,\,sat}$ at equilibrium can be expressed as

$$\bar{i}_{d,\,sat,\,eq} = \frac{1}{D_{eq}L} KN^2\omega^{*2}(\rho_{eq} - 1) < 0 \tag{20}$$

where $D_{eq} = N^2\omega^{*2} + (R^2/L^2)$.

The quasisteady-state d-axis current in (20), $\bar{i}_{d,\,sat,\,eq}$, as generated by our reduced controller when voltage saturation occurs, is an optimal $\bar{i}_d$ that satisfies both the loading condition in the mechanical subsystem and the saturated voltage constraint in the inverter. To prove this result, we consider the full model (1) and (2) operating at constant speed and constant d–q currents

$$\bar{i}_q = \frac{2B}{3KN}\omega^* + \frac{2C}{3KN}\,\mathrm{sgn}(\omega^*) \tag{21}$$

$$\begin{cases} v_d = R\bar{i}_d - LN\omega^*\bar{i}_q \\ v_q = LN\omega^*\bar{i}_d + R\bar{i}_q + KN\omega^* \end{cases} \tag{22}$$

and solve the following problem [21]:

maximize

$$\bar{i}_d$$

subject to

$$\frac{3KN}{2}\bar{i}_q - B\omega^* - C\mathrm{sgn}(\omega^*) = 0$$
$$v_d^2 + v_q^2 \le V_{sat}^2.$$

According to our results, the two extremums are on the boundary of saturated voltage constraint, and the optimal value of $\bar{i}_d$ is derived as follows:

$$\bar{i}_{d,\,opt} = \frac{1}{D_{eq}L} KN^2\omega^{*2} \times \left(\sqrt{\frac{V_{sat}^2 - \dfrac{(L^2N^2\omega^{*2} + R^2)A^2}{R^2}}{K^2N^2\omega^{*2}\left(1 - \dfrac{R^2}{L^2N^2\omega^{*2} + R^2}\right)}} - 1 \right). \tag{23}$$

Because $\bar{i}_{d,\,opt}$ in (23) is equal to $\bar{i}_{d,\,sat,\,eq}$ in (20), we can conclude that the reduced controller proposed herein automatically becomes a flux-weakening controller when voltage saturation occurs. In addition, the generated steady-state demagnetizing current, $\bar{i}_{d,\,sat,\,eq}$, is also optimal in the sense of minimum power dissipation.

The effect of $\bar{i}_{d,\,sat,\,eq}$, as generated by the reduced controller when saturation occurs, can be further explained through a d–q current figure. Consider the two sets of equations (21) and (22). For a given set of electrical parameters, (R, L, K, N), and input conditions, (v_d, v_q), only a unique set of currents, ($\bar{i}_d$, $\bar{i}_q$), satisfies (22) when the motor speed is fixed at a constant. However, when the motor speed is sufficiently high such that voltage saturation occurs and $v_d^2 + v_q^2 = V_{sat}^2$, the solutions of (22) can be plotted as a parabola, as shown in Fig. 6 which employs the motor parameters listed in Table I. The shaded area under the parabola in Fig. 6 denotes all solutions of (22) that satisfy the voltage constraint $v_d^2 + v_q^2 \le V_{sat}^2$. Notably,

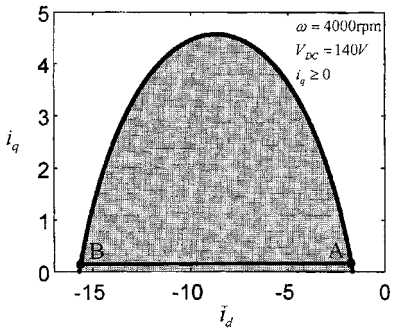

Fig. 6. Voltage-limit curve for the PMSM.

the shaded area in Fig. 6 is generated from the model of the electrical subsystem (22) under the voltage constraint alone. On the other hand, the model of the mechanical subsystem (21) dictates that $\bar{i}_q$ is a constant. Hence, the solutions of (21) and (22) can be plotted as a segment of a straight line, $\overline{\mathrm{AB}}$, in Fig. 6. The intersections of this line segment and the parabola at point A and point B depict the solutions of (21) and (22) when the voltage saturation occurs. From the results of (20) and (23) we can infer that when voltage saturation occurs continuously, control law (7), (10) combined with the adopted overmodulation strategy (12), (13) forces the operation point to stop at point A in Fig. 6 although the $\bar{i}_d^*$ is set at zero. Furthermore, the $\bar{i}_d$ value of point A in Fig. 6 depends only on the motor parameters and the saturated voltage. As a result, we can infer that under the prerequisite of stable control neither the parameters nor the gains in the controllers can affect the $\bar{i}_d$ value of point A in Fig. 6.

V. Simulation Results

The performance of the proposed controller is first verified through velocity tracking simulations. The parameters of the model of the simulated motor are identified from the motor used in the experimentation in the next section. Table I lists the parameters. Simulations are performed under four different conditions.

i) An ideal normal operating condition assumes that the motor parameters are identified correctly, and the input voltage is not saturated.
ii) Although an ideal operating condition assumes that the motor parameters are identified correctly, the input voltage is saturated in a high-speed region.
iii) Inexact motor parameters are used in the controller to examine the robustness of parameter uncertainty of the controller. In this case, the inertia, J, the winding resistance, R, and the motor constant, K, in the controller are chosen to be 50%, 50% and 105%, respectively, of the values used in the simulated motor. In addition, this simulation assumes that the motor is under normal operation and the input voltage is not saturated.
iv) The parameters in the controller are the same as in iii). However, the input voltage is saturated in a high-speed region.

The dc link voltage is set at 180 V when the simulation conditions dictate that voltage saturation should not occur, and at

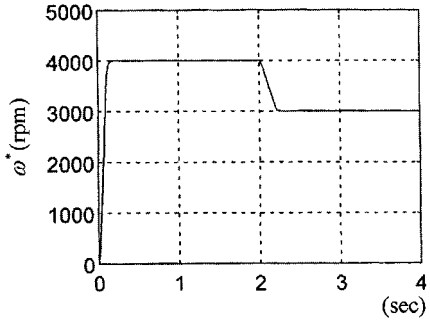

Fig. 7. Trajectory of the velocity command.

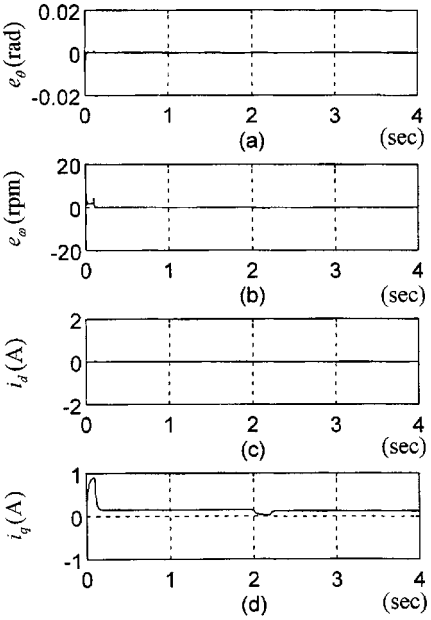

Fig. 8. Results of the tracking simulation with the reduced-order controller which contains exact motor parameters. dc link voltage is $V_{DC} = 180$ V. (a) position error, (b) velocity error, (c) d-axis current, and (d) q-axis current.

140 V for the simulations that voltage saturation is desired in a high-speed region. When the dc link voltage is set at 140 V, overmodulation continuously occurs at a high speed (exceeding 3311 rpm) for this simulated PMSM. The velocity command, as illustrated in Fig. 7, is a composite trapezoidal trajectory with two constant speed regions: one at 4000 rpm and the other at 3000 rpm. The position command is the integration of the velocity command. In all the simulations, the sampling rate is 5 kHz, and the three equivalent control gains are chosen to have equal values at $\sigma_a = \sigma_b = \sigma_c = 35 \times 2\pi$.

Figs. 8–11 summarize the simulation results under the above four conditions. According to Figs. 8(a) and (b) and 10(a) and (b), the position error and the velocity error have converged to zero under normal operation. However, the response of i_d in these simulations must be more closely examined. The value of i_d when its dynamics disappears is equivalent to the quasi-steady-state d-axis current $\bar{i}_d$. According to (5) and (7), $\bar{i}_d = \bar{i}_d^* = 0$ as long as the parameters (R, L, K) in the controller are equivalent to the real electrical parameters of the motor. This finding correlates with the simulation result in Fig. 8(c), where the controller parameters are assumed to be correct. Also,

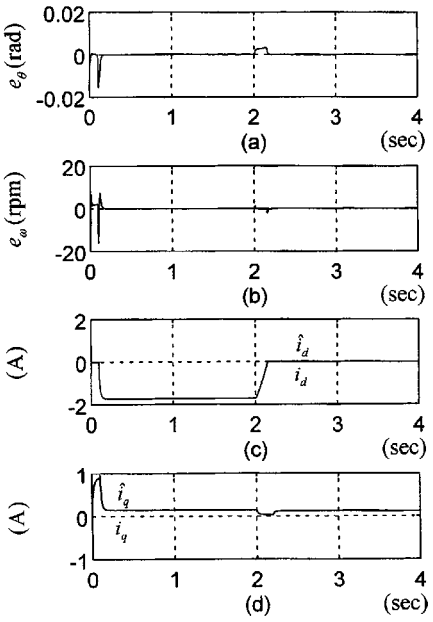

Fig. 9. Results of the tracking simulation with the reduced-order controller which contains exact motor parameters. dc link voltage is $V_{DC} = 140$ V. (a) position error, (b) velocity error, (c) d-axis current and estimated d-axis current, and (d) q-axis current and estimated q-axis current.

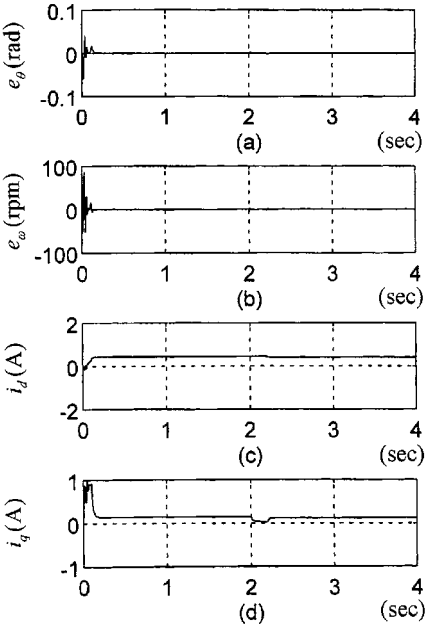

Fig. 10. Results of the tracking simulation with the reduced-order controller which contains inexact motor parameters. dc link voltage is $V_{DC} = 180$ V. (a) position error, (b) velocity error, (c) d-axis current, and (d) q-axis current.

$\bar{i}_d$ strays from zero as illustrated in Fig. 10(c), where the electrical parameters used in the controller are inexact. Additional sensitivity analysis, as shown in Fig. 12, indicates that among the three electrical parameters, $\bar{i}_d$ is the most sensitive to the magnet constant K. Consequently, if high precision control of the steady-state d-axis current is demanded, accurate identification of the electrical parameters, especially the magnet constant K, is required before implementing the proposed control. Nevertheless, according to [22], the magnet constant K can be

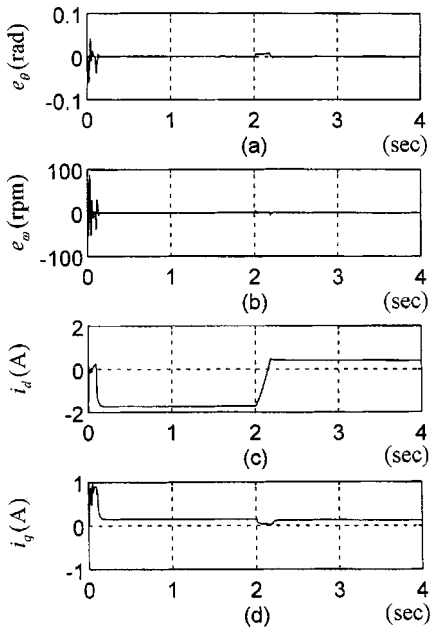

Fig. 11. Results of the tracking simulation with the reduced-order controller which contains inexact motor parameters. dc link voltage is $V_{DC} = 140$ V. (a) position error, (b) velocity error, (c) d-axis current, and (d) q-axis current.

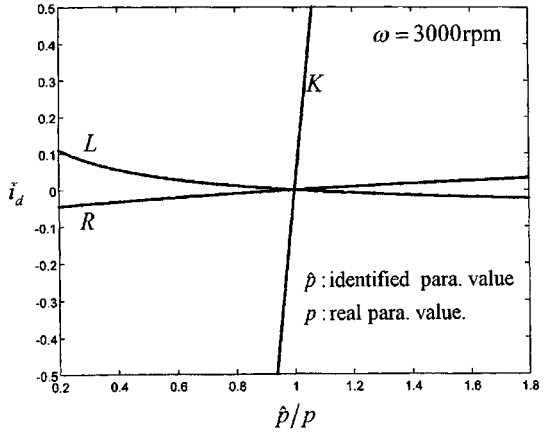

Fig. 12. Sensitivity of $\bar{i}_d$ with respect to electrical parameters.

identified the most accurately among the three electrical parameters by using the batch least-square method. Additionally, if precise electrical parameters are given, the d-axis and the q-axis currents can be estimated by constructing a simple current estimator from (5):

$$\begin{cases} \hat{i}_d(k) = \dfrac{1}{D(k)L}\{[v_q(k-1) - KN\omega(k)]N\omega(k) \\ \qquad\qquad +Rv_d(k-1)/L\} \\ \hat{i}_q(k) = \dfrac{1}{D(k)L}\{-[v_d(k-1) + KR/L]N\omega(k) \\ \qquad\qquad +Rv_q(k-1)/L\} \end{cases} \tag{24}$$

where k represents the index of the sampling sequence, and $\hat{i}_d$ and $\hat{i}_q$ are the estimated values of i_d and i_q, respectively. Fig. 9(c) and (d) illustrate the simulation results of this current estimator. It is possible to use these estimated currents as a software indicator for over current in the motor and the driver.

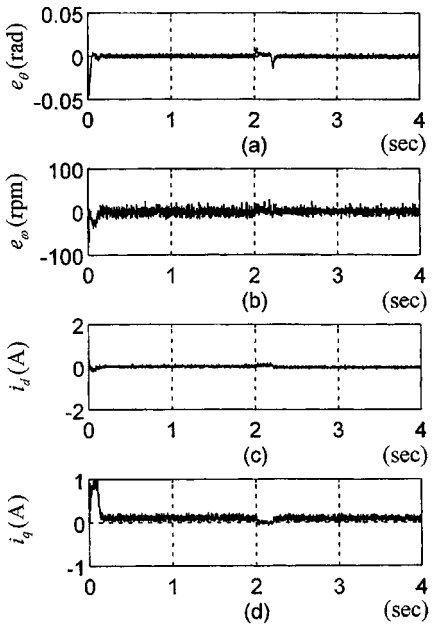

Fig. 13. Results of the tracking experiment with the reduced-order controller, whose steady-state d-axis current command is $\bar{i}_d^* = 0$. dc link voltage is $V_{DC} = 180$ V. (a) position error, (b) velocity error, (c) d-axis current, and (d) q-axis current.

When voltage saturation occurs, the position error and the velocity error also converge to zero, as shown in Figs. 9(a) and (b) and 11(a) and (b). However, the transient errors are larger than that at normal operation. Fig. 9(c) reveal that, although the d-axis current command is zero, i_d decreases to a negative value automatically at high speed and returns to zero at low speed. Moreover, by comparing i_d at the voltage saturation region in Figs. 9(c) and 11(c), the two negative steady-state i_d, or the so called demagnetizing currents, have the same value. This finding implies that the steady-state demagnetizing current under our control law is independent of the system parameters used in the controller.

Although this study is focused on SPMSM's, additional simulations indicate that, by using the proposed control method, we are able to achieve automatic flux-weakening control for interior permanent magnet synchronous motors (IPMSM's) as well.

VI. Experimental Results

The experimental setup includes a Sinano #7CB30-2SE6F permanent magnet synchronous motor, the power stage of a Micro Trend UT90 driver, a proprietary control card made in-house, and a PC. The control card converts the analog phase current measurements into digital signals, decodes the encoder signals, and generates space vector pulse width modulation (SVPWM) switching signals to control the power stage. The PC is then used to compute the control algorithms and the coordinate transformations among the vector space, the stator reference frame, and the rotor reference frame. Notably, the current measurements herein are only used to monitor the current responses. They are not used for control purposes. The experimental conditions resemble those in the tracking simulation, except that the identified motor parameters, as shown in Table I, are used in the controllers. Figs. 13 and 14

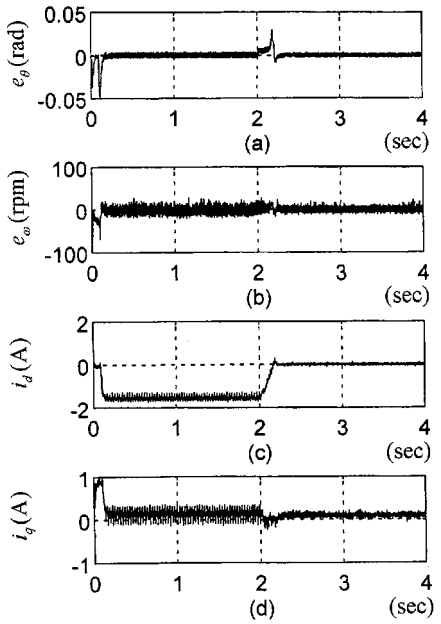

Fig. 14. Results of the tracking experiment with the reduced-order controller, whose steady-state d-axis current command is $\bar{i}_d^* = 0$. dc link voltage is $V_{DC} = 140$ V. (a) position error, (b) velocity error, (c) d-axis current, and (d) q-axis current.

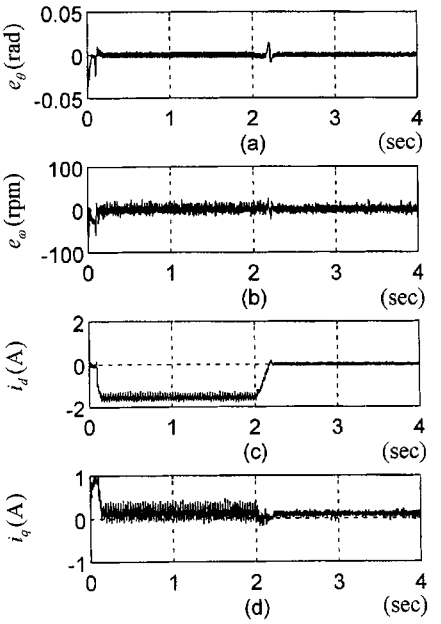

Fig. 15. Results of the tracking experiment with the reduced-order controller, whose steady-state d-axis current command is the auto-adjusting command. dc link voltage is $V_{DC} = 140$ V. (a) position error, (b) velocity error, (c) d-axis current, and (d) q-axis current.

summarize the experimental results under dc link voltage that is set at 180 V and 140 V, respectively. Under normal operation, both the position error and the velocity error converge to zero, and $\bar{i}_d$ is also approximately zero, as exhibited in Fig. 13. When voltage saturation occurs, Fig. 14(c) indicates that the phenomenon of auto-flux-weakening indeed appears in the experiment. Consequently, both the position error in Fig. 14(a) and the velocity error in Fig. 14(b) can still converge to zero at voltage saturation operation. However, the transient errors are larger than that at normal operation. This phenomenon has been predicted from the eigenvalue analysis for voltage saturation operation in Fig. 5. According to that analysis, reducing the degree of voltage saturation can reduce the transient errors and increase the control robustness in voltage saturation region. The fact that i_d approaches its optimal value $\bar{i}_{d,\,sat,\,eq}$ automatically whenever voltage saturation occurs allows us to modify the command current $\bar{i}_d^*$ in (7) to reduce the degree of voltage saturation. As a result, we set $\bar{i}_d^*$ according to the following rules:

$$\bar{i}_d^*(k+1) = \bar{i}_d^*(k) + g_{sat}\left[V_{sat} - \sqrt{v_d^2(k) + v_q^2(k)}\right]; \quad \text{if } (\bar{i}_d^*(k+1) > 0) \qquad \bar{i}_d^*(k+1) = 0 \tag{25}$$

where g_{sat} denotes a positive overmodulation tuning gain, and the initial $\bar{i}_d^*$ value is set to zero. In (25), $\bar{i}_d^*$ is modified as the integration of the degree of overmodulation when voltage saturation occurs. Consequently, $\bar{i}_d^*$ varies until voltage saturation stops, or equivalently, controller returns to normal operation. Fig. 15 presents the new experimental results with the modified control law. Apparently, the control performance is improved.

Since phase currents are not measured in this study, the protection of the motor and the driver from overloading must be implemented using other methods. For example, the current estimator (24) can be used as a software indicator for over current if the motor parameters are accurately known. Other hardware-oriented methods include the installation of a simple protection device or circuit, e.g., fuse, or a current-sensing resistance, which is much cheaper than a Hall current sensor, in the dc link bus. This idea comes form the fact that the current flowing in the dc link bus at any time is always the maximum phase current among the three phase windings when they are connected in a wye configuration. Consequently, there is no need to measure the current in the individual winding.

VII. Conclusion

This study applies the singular perturbation method to design a position and velocity controller for a SPMSM control system. The controller proposed herein is computationally simple and does not require the measurement of current signals for the feedback purposes. Consequently, the cost of the motor driver can be reduced. On the other hand, although this controller is designed without current-loop control, the steady-state current $\bar{i}_d = 0$ can still be demanded indirectly under normal operation to reduce the copper loss. Moreover, this controller automatically generates a flux-weakening control to follow the velocity command when the voltage saturation occurs, and the demagnetizing current $\bar{i}_d$ is optimal in the sense of minimum power dissipation. As a result, this controller can always achieve near-minimum power dissipation both during normal operation and voltage saturation operation. Simulation and experimental results show that the controller can achieve effective variable-speed and position control with near-minimum power dissipation, even when voltage saturation occurs.

REFERENCES

[1] J. H. Lang, G. C. Verghese, and M. Ilic-Spong, "Opportunities in estimation and control of electrical machines," in *Proc. 25th CDC*, Athens, Greece, Dec. 1986.

[2] K.-K. Shyu and H.-J. Shieh, "A new switching surface sliding-mode speed control for induction motor drive systems," *IEEE Trans. Power Electron.*, vol. 11, pp. 660–667, July 1996.

[3] F.-J. Lin, S.-L. Chiu, and K.-K. Shyu, "Novel sliding mode controller for synchronous motor drive," *IEEE Trans. Aerosp. Electron. Syst.*, vol. 34, pp. 532–542, Apr. 1998.

[4] M. Ilic- Spong, R. Marino, S. M. Peresada, and D. G. Taylor, "Nonlinear control of switched reluctance motors in robotics applications," in *Conf. Appl. Motion Contr.*, Minneapolis, MN, 1986, pp. 129–136.

[5] A. Kaddouri, O. Akhrif, H. Le-Huy, and M. Ghribi, "Nonlinear feedback control of a permanent magnet synchronous motors," in *Proc. Can. Conf. Electrical Computer Eng.*, vol. 1, 1994, pp. 77–80.

[6] D. I. Kim, I. J. Ha, and M. S. Ko, "Control of induction motors via feedback linearization with input–output decoupling," *Int. J. Contr.*, vol. 51, pp. 863–883, Apr. 1990.

[7] M. Bodson, J. N. Chiasson, R. T. Novotnak, and R. B. Rekowski, "High-performance nonlinear feedback control of a permanent magnet stepper motor," *IEEE Trans. Contr. Syst. Technol.*, vol. 1, pp. 5–14, Mar. 1993.

[8] M. Zribi and J. Chiasson, "Position control of a PM stepper motor by exact linearization," *IEEE Trans. Automat. Contr.*, vol. AC-36, pp. 620–627, May 1991.

[9] R. B. Sepe and J. H. Lang, "Real-time adaptive control of the permanent-magnet synchronous motor," *IEEE Trans. Ind. Applicat.*, vol. 27, pp. 706–714, July/Aug. 1991.

[10] R. Marino, S. Peresada, and P. Tomei, "Nonlinear adaptive control of permanent magnet step motors," *Automatica*, vol. 31, pp. 1595–1604, Nov. 1995.

[11] R. Marino, S. Peresada, and P. Vagili, "Adaptive partial feedback linearization of induction motors," in *Proc. CDC'90*, Honolulu, HI, 1990.

[12] S. Morimoto, Y. Takeda, T. Hirasa, and K. Taniguchi, "Expansion of operating limits for permanent magnet by current vector control cnsidering inverter capacity," *IEEE Trans. Ind. Applicat.*, vol. 26, pp. 866–871, Sep./Oct. 1990.

[13] S. Morimoto, Y. Takeda, and T. Hirasa, "Flux-weakening control method for surface permanent magnet synchronous motors," in *Proc. IPEC*, Tokyo, Japan, 1990, pp. 942–949.

[14] J. Shi and Y.-S. Lu, "Field-weakening operation of cylindrical permanent-magnet motors," in *Proc. IEEE Int. Conf. Contr. Applicat.*, Dearborn, Ml, Sept. 1996, pp. 864–869.

[15] A. Verl and M. Bodson, "Torque maximization for permanent magnet synchronous motors," *IEEE Trans. Contr. Syst. Technol.*, vol. 6, pp. 740–745, Nov. 1998.

[16] S. D. Sudhoff, K. A. Corzine, and H. J. Hegner, "A flux-weakening strategy for current-regulated surface-mounted permanent-magnet machine drives," *IEEE Trans. Energy Conv.*, vol. 10, pp. 431–437, Sept. 1995.

[17] J.-H. Song, J.-M. Kim, and S.-K. Sul, "A new robust SPMSM control to parameter variations in flux weakening region," *IEEE IECON*, vol. 2, pp. 1193–1198, 1996.

[18] P. V. Kokotovic, H. K. Khalil, and J. O'Reilly, *Singular Perturbation Methods in Control: Analysis and Design*. London, U.K.: Academic, 1986, ch. 1.

[19] H. K. Khalil, *Nonlinear Systems*, 2nd ed. Englewood Cliffs, NJ: Prentice-Hall, 1996, ch. 9.

[20] J.-K. Seok and S.-K. Sul, "A new overmodulation strategy for induction motor drive using space vector PWM," in *Proc. IEEE APEC*, vol. 1, Dallas, TX, Mar. 1995, pp. 211–216.

[21] J. Gregory and C. Lin, *Constrained Optimization in the Calculus of Variations and Optimal Control Theory*. New York: Van Nostrand Reinhold, 1992, ch. 1.

[22] A. J. Blauch, M. Bodson, and J. Chiasson, "High-speed parameter estimation of stepper motors," *IEEE Trans. Contr. Syst. Technol.*, vol. 1, pp. 270–279, Dec. 1993.

Jiunn-Jiang Chen was born in Kaohsiung, Taiwan, R.O.C., on May 14, 1972. He received the B.S. degree from National Chiao-Tung University, Hsinchu, Taiwan, in 1995, where he is currently pursuing the Ph.D. degree.

His research interests include power electronics and high-performance electrical machine control.

Kan-Ping Chin (S'89–M'92) was born in Taipei, Taiwan, R.O.C. He received the B.S. degree in mechanical engineering from National Taiwan University, Taipei, in 1982 and the S.M. and the Ph.D. degrees from the Massachusetts Institute of Technology, Cambridge, in 1988 and 1991, respectively.

He is now an Associate Professor at the National Chiao-Tung University, Hsinchu. His research interests include control of servo motors and the microelectromechanical systems (micromotors).